RUKA-V2: Tendon-Driven Open-Source Dexterous Hand with Wrist and Abduction for Robot Learning

Anonymous Authors

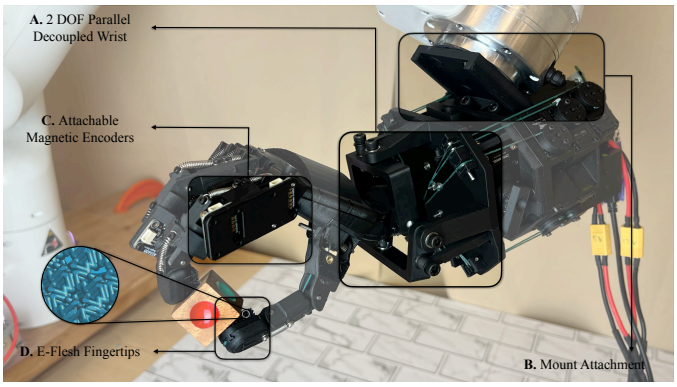

Fig. 1: (**A**) RUKA-V2 has an integrated 2-DOF decoupled parallel wrist and finger abduction/adduction. (**B**) Side-mounted wrist attachment for easy integration with table-top manipulators. (**C**) Attachable magnetic encoders for joint angle calibration. (**D**) E-flesh fingertips [1] for softer, compliant grip with optional tactile sensing. All components are open-sourced.

***Abstract*—Lack of accessible and dexterous robot hardware has been a significant bottleneck to achieving human-level dexterity in robots. Previously, we released RUKA, a fully open-sourced, tendon-driven humanoid hand with 11 degrees of freedom, buildable for under $1,300. Despite its contributions, RUKA lacked wrist mobility and finger adduction/abduction—two degrees of freedom essential for imitating human behavior. In this paper, we introduce RUKA-V2: a fully open-sourced, tendon-driven humanoid hand featuring a decoupled 2-DOF parallel wrist and abduction/adduction at the fingers. The parallel wrist enables manipulation in confined environments such as cabinets, while abduction enables motions such as grasping thin objects and calligraphy. We evaluate RUKA-V2 against RUKA through user studies on teleoperated tasks, finding a 51.3% reduction in completion time and a 21.2% increase in success rate. We further demonstrate teleoperation across 13 dexterous tasks and autonomous policy learning on 3 tasks. All design files, assembly instructions, and software are open-sourced.**

***Index Terms*—dexterous manipulation, humanoid hand, tendon-driven, robot learning, teleoperation**

I. INTRODUCTION

Human hands possess over 20 degrees of freedom (DOF), a 3-DOF wrist, distributed tactile sensing, and a compliant form factor [2]–[4]. Replicating this dexterity in robotic hardware remains a major bottleneck, despite significant algorithmic progress in manipulation [5]–[8].

Direct-driven hands such as Allegro [9] and LEAP [10] are widely used but bulky and require significant effort to close the embodiment gap [11]–[14]; smaller direct-driven alternatives either overheat quickly [15] or cost around $50,000 [16]. Tendon-driven designs [17]–[24] move actuators to the forearm for compactness, but hands like the Shadow Hand [24] cost over $100,000 while more accessible options are limited in DOF [19], [25], not fully open-sourced [23], or lack documentation [18], [20]–[22], [26]. Notably, despite humans relying heavily on wrist motion, most designs focus on the fingers rather than the wrist.

Building on RUKA [17], we introduce RUKA-V2: a tendon-driven humanoid hand with a decoupled parallel 2-DOF wrist and finger abduction/adduction. Our contributions are:

1) A 2-DOF parallel wrist and abduction/adduction mechanism that yields a 51.3% reduction in teleoperation task completion time and 21.2% increase in task success rate over RUKA in user studies (Section IV-B).
2) A set of design principles for robot learning hardware, including side-mounted wrist attachments for table-top manipulators and 3D-printed E-flesh [1] fingertips for compliant grip without silicone molding.
3) Attachable magnetic encoders for joint angle calibration, removing the need for expensive motion capture gloves.

We open-source all software, 3D printable files, and documentation supported by instructional videos, teleoperate RUKA-V2 across 10 single-arm and 3 bimanual dexterous tasks including writing, and demonstrate learned autonomous policies on 3 tasks. A comparison to other hands is provided in Table I.

Collectively, we believe that Ruka-v2 will serve as a valuable tool for dexterous manipulation research, both for algorithmic development and, with modifiable CAD files, for hardware research as well. We provide a thorough comparison of Ruka-v2 to other listed robot hardware in Table 1. All hardware and software components, along with robot videos, are open-sourced.

II. HARDWARE DESIGN

RUKA-V2 builds on RUKA by adding two hardware capabilities critical for human-like manipulation: (i) a decoupled 2-DOF parallel wrist and (ii) controlled finger abduction/adduction. We also present an optional DIP/PIP joint coupling system and a set of attachable magnetic encoders mountable across all joints of RUKA and RUKA-V2 for calibration and joint angle sensing. All major structural components are 3D printed; bearings, fasteners, and springs are off-the-shelf. Actuators are placed proximally in the forearm to reduce distal inertia, and tendons are routed through the wrist and palm via guides that prevent sharp bends. An overview is shown in Figure 2. We

TABLE I: Comparison of dexterous robotic hands. **Open-source**: ✓ = hardware & software fully public; ∼ = partial; ✗ = proprietary. **Act.**: T = tendon; DD = direct-drive. **Tactile**: opt. = optional add-on. †HW files public; SW closed. ‡Price reported by third-party sources only. §Thermal throttling observed after ∼40 min in internal testing.

Metric	 Allegro V4	 Ruka v1	 ORCA	 Wuji Hand	 Sharpa Wave	 Unitree Dex5	 RUKA-V2 (Ours)
Open-source	∼†	✓	✓	✗	✗	✗	✓
Cost (USD)	∼$16K	∼$1.3K	∼$3.5K	∼$5.5K	∼$50K‡	∼$25K	∼$1.5K
Tot. / Act. DOF	16 / 16	15 / 11	17 / 17	20 / 20	22 / 22	21 /	20 / 16
Wrist DOF	0	0	1	0	0	0	2
Actuation	DD	T	T	DD	DD	DD	T
Hand size	∼30%larger	Human	Human	Human	Human	Human	Human
Tactile	opt.	✗	✓ (FSR)	✗	✓ (DTA)	✓ (opt.)	✓ (opt.)
Durability	High	High	>10K cyc.	∼40 min§	>2.5M cyc.	High	>5Hours

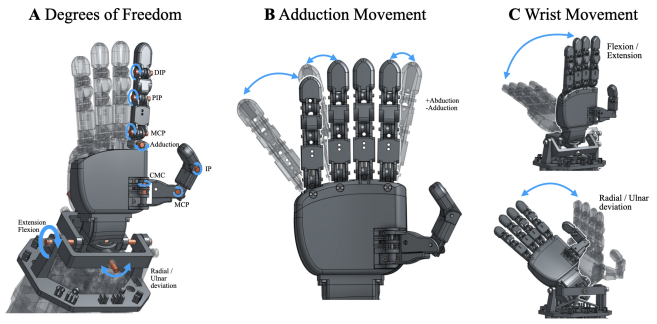

Fig. 2: **RUKA-V2 hardware overview.** (**A**) 18 DOF across fingers and thumb, plus 2 DOF wrist. (**B**) Independent knuckle module for finger abduction/adduction. (**C**) 2 DOF wrist with flexion/extension and radial/ulnar deviation via decoupled parallel linkages.

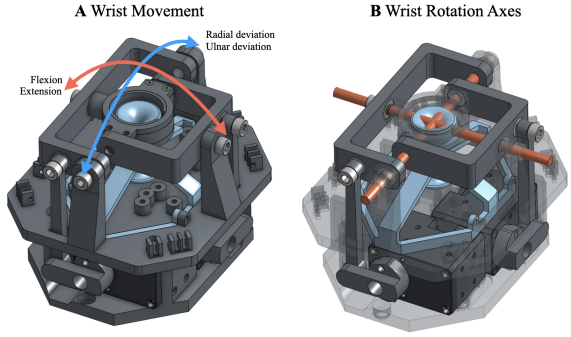

Fig. 3: **2-DOF wrist kinematics.** (**A**) Independent flexion/extension (red) and radial/ulnar deviation (blue) axes. (**B**) Intersecting axes share a spherical ball joint center; each DOF is driven by a dedicated forearm motor via a rectangular linkage.

describe each component in detail below and summarize a comparative analysis against other hands in Table I.

A. Design Principles

a) Accessibility: We open-source all design files including modifiable CAD models, with step-by-step build instructions and video tutorials. The only specialized equipment required is a 3D printer — all other components are off-the-shelf. RUKA-V2 uses E-flesh [1] fingertip attachments printed in TPU for a compliant form factor without silicone molding. Total material cost is under $1,500.

b) Reliability: The hand sustains over 5 hours of continuous operation without thermal throttling (see Appendix), and its modular open-source design enables quick in-house repairs.

B. Wrist Kinematics

Since all finger tendons must route through the wrist, designing a 2-DOF wrist that does not disturb finger motion is non-trivial. We adopt a decoupled parallel mechanism similar to [27], where flexion/extension and radial/ulnar deviation are actuated independently via rectangular linkages whose axes meet at a single pivot defined by a passive spherical ball joint (Figure 3). This minimizes palm translation and cross-axis coupling. A through-hole in the ball joint allows tendons to pass near the rotation center, and a bearing-supported routing plate prevents entanglement during large wrist rotations.

C. Finger Abduction/Adduction

To enable finger spacing adjustments needed for pinching thin objects and conforming to irregular geometry, RUKA-V2 adds controlled abduction/adduction at the MCP joints. Independent knuckle modules house both the primary MCP flexion axis and a secondary lateral rotation axis. Each joint is driven by a dedicated tendon from a forearm motor, while an extension spring restores the finger to neutral when relaxed (Figure 4). The middle finger remains fixed as a structural

reference. This adds compliance during contact while enforcing a well-defined default posture.

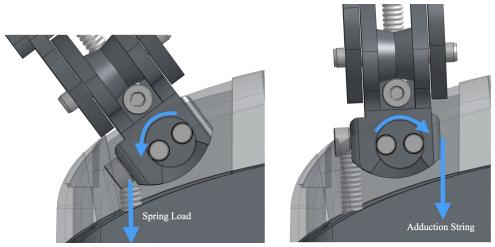

Fig. 4: **Finger abduction/adduction mechanism.** (**Left**) Extension spring pulls the finger laterally outward, providing passive compliance. (**Right**) Tendon-driven adduction rotates the knuckle inward against spring force. Blue arrows indicate force direction.

D. Optional DIP/PIP Coupling

In RUKA, the PIP and DIP joints share a single motor, but no mechanism enforces equal joint displacement, meaning that friction, slack, and wear cause the relative motion to vary across builds. RUKA-V2 provides an optional rigid coupling mechanism using fixed-length coupling strings routed through internal channels that enforce a deterministic PIP–DIP relationship (Figure 5). This improves repeatability and simplifies control at the cost of passive compliance. We evaluate the effect on motion consistency in Appendix .

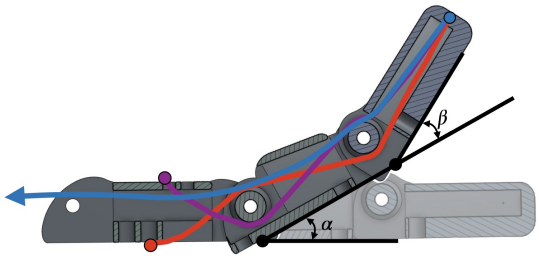

Fig. 5: **DIP–PIP coupling mechanism.** Fixed-length coupling strings (red & purple) enforce $\alpha \approx \beta$.

E. Attachable Magnetic Encoders

To evaluate joint angle accuracy without expensive motion capture gloves, we designed a set of attachable magnetic encoders using AS5600 sensors with 12-bit resolution (Figure 6). The set consists of rare earth magnet holders and 6 attachable parts for the index and thumb fingers (3 each). Magnet holders are press-fitted into joint dowel pins, and sensor structures attach using screws already part of the hand design, requiring no additional fasteners. An ESP32 QTPy microcontroller interfaces the sensors over an I2C multiplexer. These encoders can be used both for calibration and for capturing the motor–joint mapping directly, and are compatible with both RUKA-V2 and RUKA.

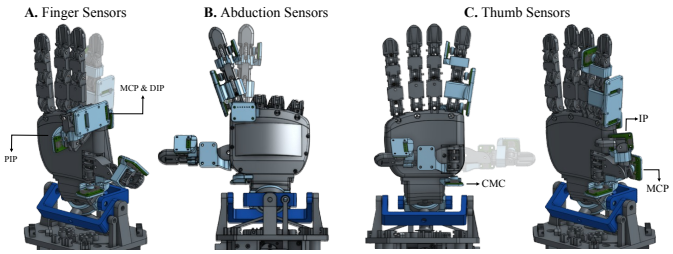

Fig. 6: **Magnetic encoder placement.** (**A**) Finger sensors for MCP, PIP, DIP. (**B**) Abduction sensor on the back. (**C**) Thumb CMC, MCP, and IP sensors.

F. Range of Motion

Table II compares the per-joint range of motion of RUKA-V2 against human values. RUKA-V2 meets or exceeds human range of motion on most joints; the wrist range is smaller but sufficient for the target manipulation tasks.

TABLE II: Range of motion (↑) of RUKA-V2 vs. human [4]. ✓ = meets/exceeds human; ∼ = DOF exists but range not reached; ✗ = DOF absent.

Type	Joint	Human	RUKA-V2	Pass
Fingers	DIP	85°	120°	✓
	PIP	105°	120°	✓
	MCP	85°	140°	✓
Thumb	IP	80°	120°	✓
	MCP	56°	90°	✓
	CMC	−−	170°	✓
Abd./Add.	Index	20–25°	20°	✓
	Middle	10–12°	Fixed	✗
	Ring	20–25°	23°	✓
	Pinky	30–35°	45°	✓
Wrist	Flexion	80–90°	45°	∼
	Extension	70°	30°	∼
	Radial dev.	20°	35°	✓
	Ulnar dev.	30°	35°	✓

III. APPLICATIONS OF RUKA-V2

We hope that RUKA-V2 will serve as a suitable research tool for robot learning. To evaluate its usability, we implement a joint-space controller, teleoperate RUKA-V2 across 10 single-arm tasks and 3 bimanual tasks, and train robot policies for 3 tasks. We describe each component below. The full software stack including the controller and calibration is open-sourced.

A. Controller

For tendon-driven hands, the mapping between joint angles and motor values is non-trivial. RUKA introduced a data-driven approach but relied on expensive motion capture gloves. In RUKA-V2, we decouple retargeting and joint-to-motor mapping. Similar to [23], we define a linear mapping between joint angles $\theta \in [\theta_{\min}, \theta_{\max}]$ and motor positions $p \in [p_{\min}, p_{\max}]$:

$$p = p_{\min} + c \cdot \frac{\theta}{\theta_{\max} - \theta_{\min}} \cdot (p_{\max} - p_{\min})$$

where c compensates for tendon friction and finger weight. Motor limits are determined via automated calibration: $p_{\min}$ corresponds to initial tendon tensioning and $p_{\max}$ to the mechanical limit. For retargeting, we adopt AnyTeleop's [14] vector-based Dex Retargeting module, which optimizes robot joint angles to align RUKA-V2's link vectors with human finger directions extracted from a video stream.

B. Teleoperation

We mount RUKA-V2 on a 7-DOF Franka arm and use the Open Teach framework [28] with an Oculus VR headset for teleoperation. Wrist trajectories from the headset are mapped to the Franka arm's end-effector via inverse kinematics, and hand poses are passed through our controller to generate motor commands. For bimanual tasks, we synchronize two identical Franka arm setups. We perform 10 single-arm tasks and 3 bimanual tasks (see Figures 12 and 13 in the Appendix).

C. Policy Learning

We use the BAKU [29] framework to train policies for three tasks: bread pick-and-place, opening a music box, and pen grasping using abduction/adduction. Approximately 100 teleoperated demonstrations per task are collected, with Gaussian noise injected into joint states [30] to enrich recovery behaviors. The observation space includes 23-dimensional proprioception state (7-DOF Franka + 16-DOF RUKA-V2) encoded with an MLP concatenated with an RGB stream encoded via ResNet-18 [31], which are fed through a transformer-based [32] trunk and an action chunking head to predict a sequence of future actions. We evaluate at 10 random initial positions per task with 5 rollouts each (see Figure 14 in the Appendix).

IV. EXPERIMENTAL EVALUATION

We evaluate RUKA-V2 through controller accuracy measurements using the attachable encoders and a user experience study comparing it against RUKA. Additional experiments on thermal endurance, payload capacity, and DIP/PIP coupling are provided in the Appendix.

A. Controller Accuracy

Using the attachable magnetic encoders (Section II-E), we evaluate the accuracy of our linear controller (Section III-A) by sampling 20 random target angles per joint within its limits, commanding the joint to the corresponding motor positions using the controller, and measuring the absolute error between commanded angles $\theta_{expected}$ and ground truth readings θ_{actual}. Each position was held for 1.5 seconds before measurement. We report both absolute error and normalized error as a percentage of each joint's range.

Table III summarizes the results. The overall average error is 8.26° (10.68% of joint range). The thumb IP joint achieves the lowest error (2.76°), while the index MCP joint shows the highest (12.77°), likely due to greater tendon friction at the proximal joints. Despite the simplicity of the linear mapping, these errors are within a usable range for teleoperation and policy learning, as demonstrated by the task success rates in our user study and policy evaluations.

TABLE III: Average joint angle tracking error for RUKA-V2.

Joint Name	Avg. Error (°)	Avg. Error (%)
Index Abduction	3.76	15.96%
Index DIP	7.69	9.62%
Index PIP	11.91	11.91%
Index MCP	12.77	8.51%
Thumb CMC	7.85	7.47%
Thumb MCP	11.07	16.27%
Thumb IP	2.76	5.01%
Overall Average	**8.26°**	**10.68%**

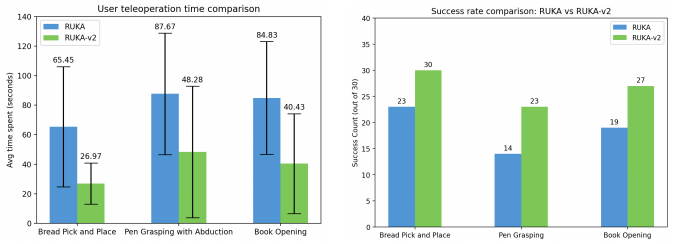

(a) Task completion time (b) Task success rate

Fig. 7: **RUKA vs. RUKA-V2 user study.** We observe a 51.3% reduction in completion times and 21.2% increase in success rate across all tasks.

B. RUKA *vs.* RUKA-V2 *User Experience*

To evaluate usability, we conducted a user study with 10 participants. Each participant performed three single-arm manipulation tasks using the teleoperation setup (Section III-B) with both RUKA and RUKA-V2. After a two-minute familiarization period, participants performed three trials per task with a 120-second time limit; trials exceeding this limit were counted as failures. The tasks were:

1) **Bread Pick-and-Place:** Pick up bread and place on a plate.
2) **Pen Grasping:** Pick up a pen from a vertical pen holder using abduction/adduction.
3) **Book Opening:** Open the cover of a hard-cover book.

RUKA-V2 achieved a **51.3% reduction in mean completion time** and a **21.2% increase in overall success rate** compared to RUKA. Results are shown in Figure 7. The improvements are attributed to the added wrist mobility, which eliminates the need to reposition the entire arm for orientation changes, and abduction/adduction, which enables more natural grasping strategies.

V. DISCUSSION

We presented RUKA-V2, extending RUKA with a 2-DOF decoupled parallel wrist and per-finger abduction/adduction. We acknowledge two limitations: (1) our linear joint-to-motor mapping, while sufficiently accurate (Section IV-A), has not been formally verified — data-driven approaches using our magnetic sensors could improve this; (2) while our E-flesh fingertips support optional tactile sensing, magnetic interference between sensors requires further characterization. Future directions include non-linear controller models and seamless tactile integration.

REFERENCES

[1] V. Pattabiraman, Z. Huang, D. Panozzo, D. Zorin, L. Pinto, and R. Bhirangi, "eflesh: Highly customizable magnetic touch sensing using cut-cell microstructures," 2025. [Online]. Available: https://arxiv.org/abs/2506.09994

[2] J. Hong, L. Stearns, J. Froehlich, D. Ross, and L. Findlater, "Evaluating angular accuracy of wrist-based haptic directional guidance for hand movement," in *Proceedings of the 42nd Graphics Interface Conference*, ser. GI '16. Waterloo, CAN: Canadian Human-Computer Communications Society, 2016, p. 195–200.

[3] D. Hu, D. Howard, and L. Ren, "Biomechanical analysis of the human finger extensor mechanism during isometric pressing." *PLoS One*, vol. 9,4, 2014. [Online]. Available: doi:10.1371/journal.pone.0094533

[4] M. C. Hume, H. Gellman, H. McKellop, and R. H. Brumfield, "Functional range of motion of the joints of the hand," *The Journal of Hand Surgery*, vol. 15, no. 2, pp. 240–243, 1990. [Online]. Available: https://www.sciencedirect.com/science/article/pii/036350239090102W

[5] I. Guzey, H. Qi, J. Urain, C. Wang, J. Yin, K. Bodduluri, M. Lambeta, L. Pinto, A. Rai, J. Malik, T. Wu, A. Sharma, and H. Bharadhwaj, "Dexterity from smart lenses: Multi-fingered robot manipulation with in-the-wild human demonstrations," 2025. [Online]. Available: https://arxiv.org/abs/2511.16661

[6] C. Chi, Z. Xu, S. Feng, E. Cousineau, Y. Du, B. Burchfiel, R. Tedrake, and S. Song, "Diffusion policy: Visuomotor policy learning via action diffusion," *The International Journal of Robotics Research*, 2024.

[7] S. Haldar and L. Pinto, "Point policy: Unifying observations and actions with key points for robot manipulation," 2025. [Online]. Available: https://arxiv.org/abs/2502.20391

[8] Z. J. Cui, O. Rayyan, H. Etukuru, B. Tan, Z. Andrianarivo, Z. Teng, Y. Zhou, K. Mehta, N. Wojno, K. Y. Wu, M. H. Anjaria, Z. Wu, M. Mao, G. Zhang, B. Shah, Y. Kim, S. Chintala, L. Pinto, and N. M. M. Shafiullah, "Contact-anchored policies: Contact conditioning creates strong robot utility models," 2026. [Online]. Available: https://arxiv.org/abs/2602.09017

[9] "Allegro," 2024. [Online]. Available: https://www.allegrohand.com/ah-v4

[10] K. Shaw, A. Agarwal, and D. Pathak, "Leap hand: Low-cost, efficient, and anthropomorphic hand for robot learning," 2023. [Online]. Available: https://arxiv.org/abs/2309.06440

[11] I. Guzey, Y. Dai, G. Savva, R. Bhirangi, and L. Pinto, "Bridging the human to robot dexterity gap through object-oriented rewards," 2024. [Online]. Available: https://arxiv.org/abs/2410.23289

[12] C. Pan, C. Wang, H. Qi, Z. Liu, H. Bharadhwaj, A. Sharma, T. Wu, G. Shi, J. Malik, and F. Hogan, "Spider: Scalable physics-informed dexterous retargeting," 2026. [Online]. Available: https://arxiv.org/abs/2511.09484

[13] Z. Mandi, Y. Hou, D. Fox, Y. Narang, A. Mandlekar, and S. Song, "Dexmachina: Functional retargeting for bimanual dexterous manipulation," 2025. [Online]. Available: https://arxiv.org/abs/2505.24853

[14] Y. Qin, W. Yang, B. Huang, K. V. Wyk, H. Su, X. Wang, Y.-W. Chao, and D. Fox, "Anyteleop: A general vision-based dexterous robot arm-hand teleoperation system," 2024. [Online]. Available: https://arxiv.org/abs/2307.04577

[15] "Wuji," 2025. [Online]. Available: https://docs.wuji.tech/en/

[16] "Sharpa," 2025. [Online]. Available: https://www.sharpa.com/

[17] A. Zorin, I. Guzey, B. Yan, A. Iyer, L. Kondrich, N. X. Bhattasali, and L. Pinto, "Ruka: Rethinking the design of humanoid hands with learning," *Robotics: Science and Systems (RSS)*, 2025.

[18] J. Yuan, H. Zhu, J. Dai, and S. Yi, "Development of the bioinspired tendon-driven dexhand 021 with proprioceptive compliance control," 2025. [Online]. Available: https://arxiv.org/abs/2511.03481

[19] "Inmoov," 2012. [Online]. Available: https://inmoov.fr/inmoov-hand/

[20] K. Junge and J. Hughes, "Adapt-teleop: robotic hand with human matched embodiment enables dexterous teleoperated manipulation," 2025. [Online]. Available: https://doi.org/10.1038/s44182-025-00034-3

[21] M. V. Weghe, M. Rogers, M. Weissert, and Y. Matsuoka, "The act hand: design of the skeletal structure," *IEEE International Conference on Robotics and Automation, 2004. Proceedings. ICRA '04. 2004*, vol. 4, pp. 3375–3379 Vol.4, 2004. [Online]. Available: https://api.semanticscholar.org/CorpusID:5757508

[22] S. Puhlmann, J. Harris, and O. Brock, "Rbo hand 3: A platform for soft dexterous manipulation," *IEEE Transactions on Robotics*, vol. 38, no. 6, p. 3434–3449, Dec. 2022. [Online]. Available: http://dx.doi.org/10.1109/TRO.2022.3156806

[23] C. C. Christoph, M. Eberlein, F. Katsimalis, A. Roberti, A. Sympetheros, M. R. Vogt, D. Liconti, C. Yang, B. G. Cangan, R. J. Hinchet, and R. K. Katzschmann, "Orca: An open-source, reliable, cost-effective, anthropomorphic robotic hand for uninterrupted dexterous task learning," 2025. [Online]. Available: https://arxiv.org/abs/2504.04259

[24] "Shadow hand," 2022, shadow Hand. [Online]. Available: https://www.shadowrobot.com/dexterous-hand-series/

[25] "Tetheria," 2025. [Online]. Available: https://tetheria.ai/

[26] K. Shaw and D. Pathak, "LEAP hand v2: Dexterous, low-cost anthropomorphic hybrid rigid soft hand for robot learning," in *2nd Workshop on Dexterous Manipulation: Design, Perception and Control (RSS)*, 2024. [Online]. Available: https://openreview.net/forum?id=eQomRzRZEP

[27] M. Peticco, G. Ulloa, J. Marangola, N. Dashora, and P. Agrawal, "Dexwrist: A robotic wrist for constrained and dynamic manipulation," 2025. [Online]. Available: https://arxiv.org/abs/2507.01008

[28] A. Iyer, Z. Peng, Y. Dai, I. Guzey, S. Haldar, S. Chintala, and L. Pinto, "Open teach: A versatile teleoperation system for robotic manipulation," 2024.

[29] S. Haldar, Z. Peng, and L. Pinto, "BAKU: An efficient transformer for multi-task policy learning," in *The Thirty-eighth Annual Conference on Neural Information Processing Systems*, 2024. [Online]. Available: https://openreview.net/forum?id=uFXGsiYkkX

[30] V. Pattabiraman, Y. Cao, S. Haldar, L. Pinto, and R. Bhirangi, "Learning precise, contact-rich manipulation through uncalibrated tactile skins," 2024. [Online]. Available: https://arxiv.org/abs/2410.17246

[31] K. He, X. Zhang, S. Ren, and J. Sun, "Deep residual learning for image recognition," 2015. [Online]. Available: https://arxiv.org/abs/1512.03385

[32] A. Vaswani, N. Shazeer, N. Parmar, J. Uszkoreit, L. Jones, A. N. Gomez, L. Kaiser, and I. Polosukhin, "Attention is all you need," in *Advances in Neural Information Processing Systems 30: Annual Conference on Neural Information Processing Systems 2017, December 4-9, 2017, Long Beach, CA, USA*, 2017, pp. 5998–6008.

APPENDIX

A.1 THERMAL ENDURANCE

To evaluate thermal reliability during prolonged operation, we conducted a continuous runtime test over 5 hours. Each degree of freedom for the fingers was actuated and released fully in sequence, followed by back-and-forth motion of both wrist DOFs. Motor temperatures were recorded throughout the motions. (Figure 8).

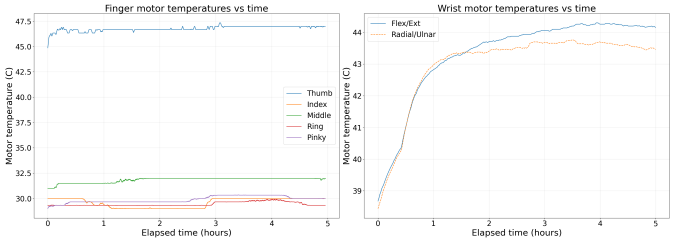

Fig. 8: **5-hour thermal endurance.** Finger motors (left) and wrist motors (right). No thermal limiting was observed.

Across all motors, temperatures increased during the initial phase (≈30 min) and then gradually approached steady state. No motor exceeded its safe operating limit, and no thermal shutdown or performance degradation was observed. The finger motors showed the lowest thermal variation (peak 30.75°C), while the wrist motors exhibited the largest excursion (peak 46.00°C, ΔT = 7.25°C) but remained within safe limits throughout (Table IV).

TABLE IV: Motor temperatures during 5-hour thermal endurance test.

Motor group	Peak (°C)	Steady (°C)	ΔT (°C)
Fingers	30.75	30.35	0.81
Thumb	47.33	46.97	1.70
Wrist	46.00	43.80	7.25

A.2 Payload

We evaluated the payload capability by measuring the maximum load that could be statically supported under different joints and wrist orientations (Figure 9). In each trial, weights were gradually added until the hand could no longer maintain the target posture.

(a) Finger DIP–PIP (b) Wrist supination (c) Wrist radial/ulnar

Fig. 9: **Payload test setup.** Static payload evaluation under three representative loading conditions.

The coupled DIP–PIP joints supported the highest load (1200 g for 15 s), while finger adduction supported 150 g, reflecting the lower stiffness of this motion direction. The wrist supported up to 1215 g in supination/pronation and 835 g in radial/ulnar orientations, indicating orientation-dependent load capacity (Table V).

TABLE V: Static payload performance.

Condition	Max load (g)	Hold (s)
Fingers DIP-PIP	1200	15
Fingers MCP	780	15
Fingers adduction	150	15
Thumb	835	20
Wrist (supination)	1215	20
Wrist (pronation)	1215	20
Wrist (radial-up)	835	20
Wrist (ulnar-up)	835	20

A.3 Controller Accuracy: Detailed Results

We test the accuracy of the linear controller by evaluating each of the 4 index finger joints and 3 thumb joints individually. 20 random angles within the joint limits are sampled and the corresponding motor commands are calculated with the controller. The motors are then moved to each position and held for 1.5 seconds for measurement. Figure 10 shows the detailed commanded vs. measured joint angle trajectories, complementing the summary in Section IV-A.

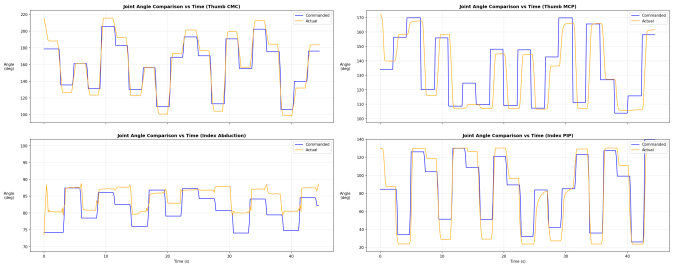

Fig. 10: **Joint angle comparison.** Expected vs. ground truth angles measured by the magnetic encoders.

A.4 DIP/PIP Coupling Effect

To evaluate the effect of the redesigned DIP–PIP coupling mechanism (Section II-D), we compared the measured joint trajectories of the previous finger design and the coupled Ruka-v2 finger under repeated flexion–extension sweeps. The index finger was driven through repeated motion cycles while the joint angle was measured against the commanded motor position.

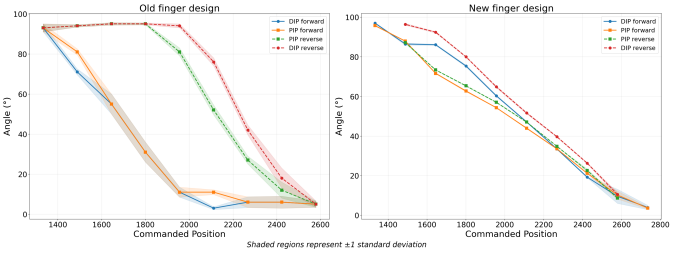

Fig. 11: **DIP–PIP coupling effect.** Previous design (left) vs. coupled mechanism (right). Shaded regions: ± 1 std across trials.

In the previous design (Figure 11, left), trajectories exhibit larger trial-to-trial variation, especially near the lower-angle region and during direction reversal, indicating stronger effects of tendon slack and friction. The redesigned coupled mechanism (right) produces more tightly clustered and repeatable trajectories, improving motion consistency for both grasp execution and controller design.

A.5 Teleoperation and Policy Learning

We teleoperate Ruka-v2 across 10 single-arm tasks and 3 bimanual tasks using the setup described in Section III-B. Single-arm tasks include writing, pen picking, charger plugging, book opening, bread grasping, opening a music box, card sliding, oven opening, and toy picking (Figure 12). For bimanual tasks, we synchronize two identical Franka arm setups and perform grasping bread from the oven, de-cluttering, and wiping a table (Figure 13). Policy rollout results for the three learned tasks are shown in Figure 14.

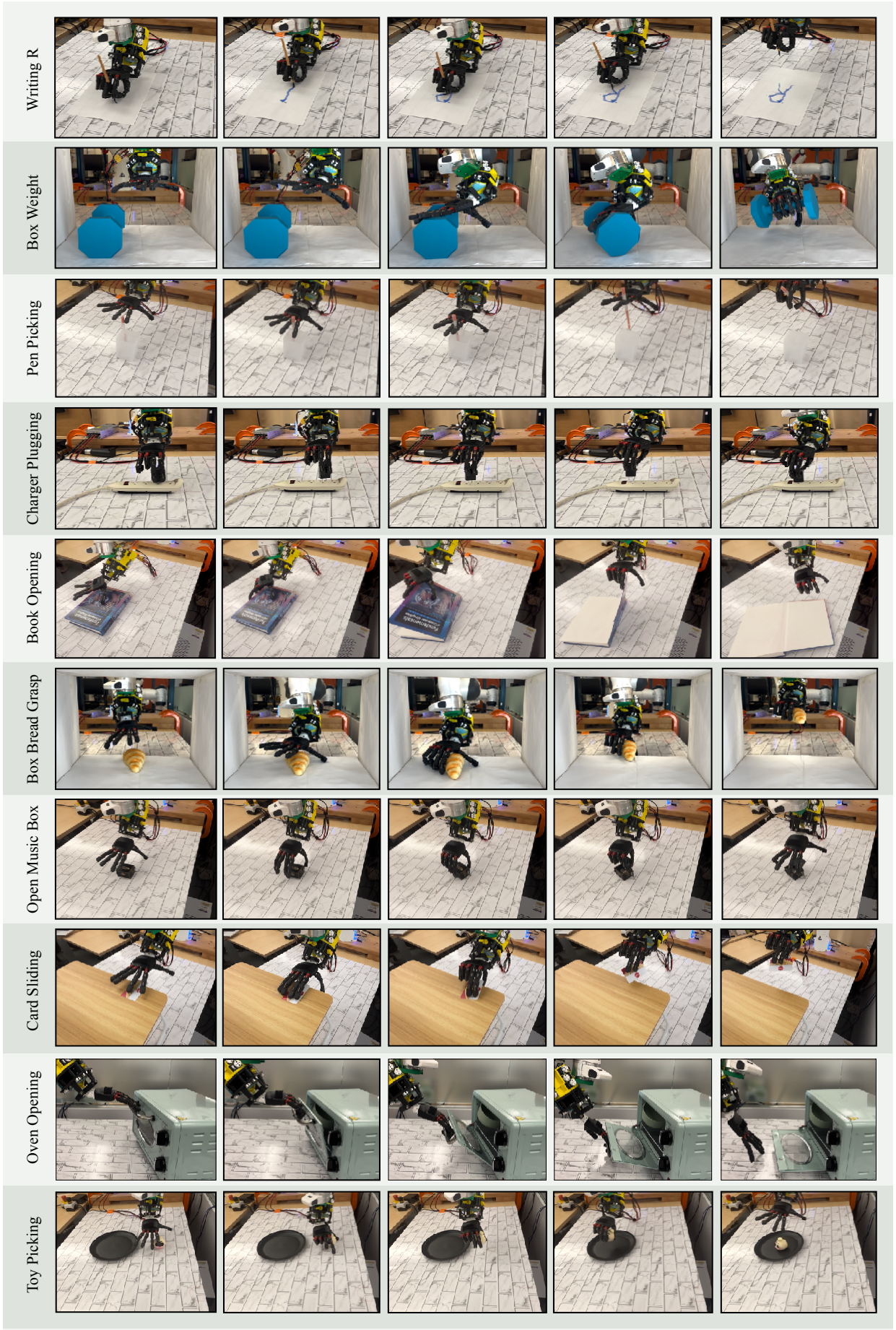

Fig. 12: **Single-arm teleoperated tasks.**

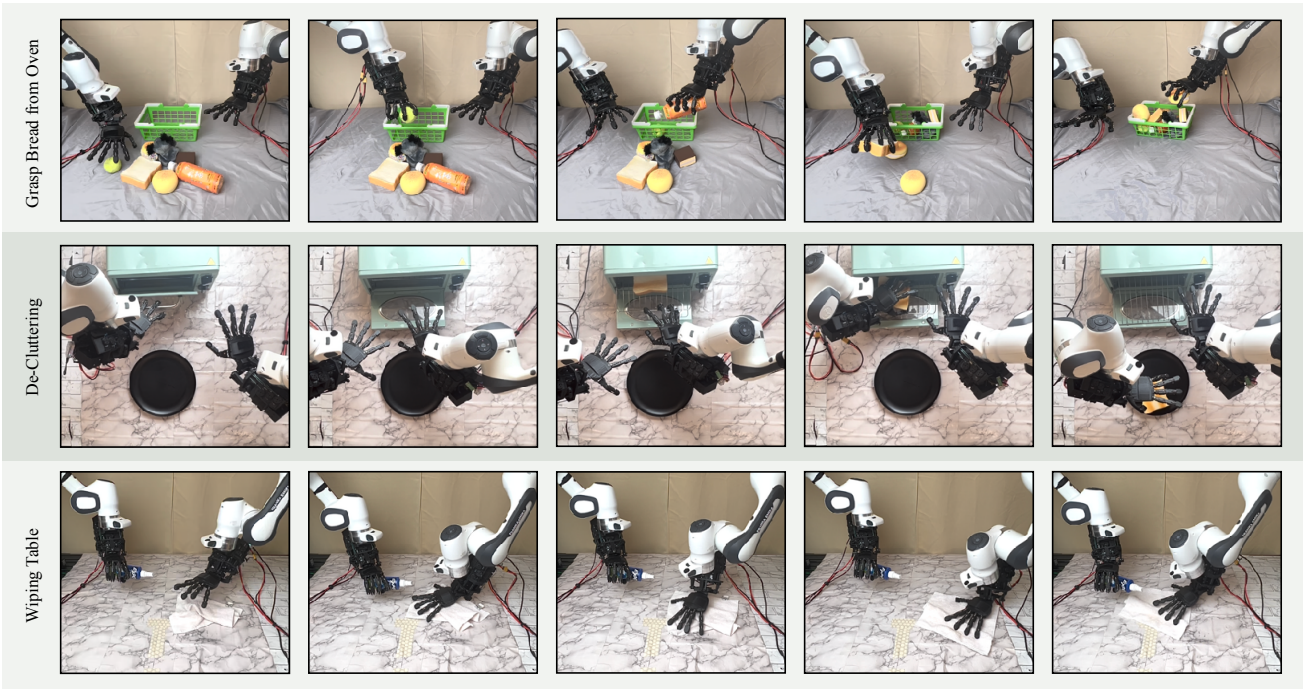

Fig. 13: **Bimanual teleoperated tasks**.

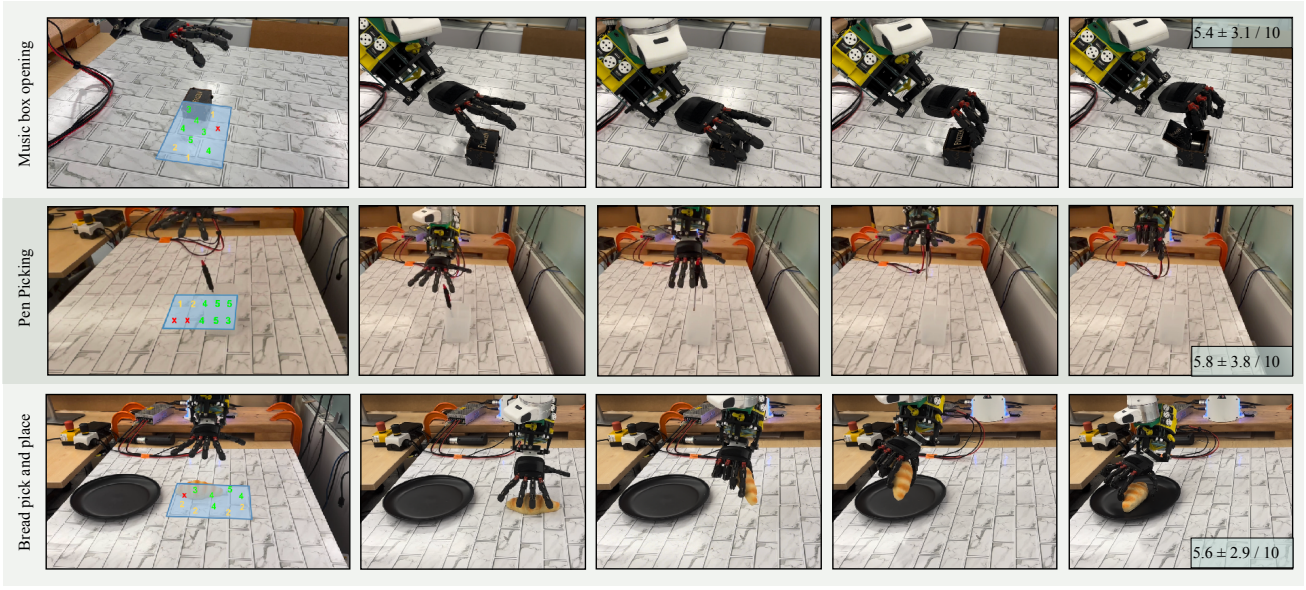

Fig. 14: **Policy rollouts.** Success rates for each starting position are reported out of 5, and total mean and standard deviation success rates are scaled to a 10 point scale.